Dopant mapping of Be δ-doped layers in GaAs tailored by counterdoping using scanning tunneling microscopy

Ph. Ebert, S. Landrock, Y. P. Chiu, U. Breuer, and R. E. Dunin-Borkowski

Citation: Appl. Phys. Lett. **101**, 192103 (2012); doi: 10.1063/1.4765360
View online: http://dx.doi.org/10.1063/1.4765360
View Table of Contents: http://apl.aip.org/resource/1/APPLAB/v101/i19
Published by the American Institute of Physics.

Dopant mapping of Be δ-doped layers in GaAs tailored by counterdoping using scanning tunneling microscopy

Ph. Ebert,[1,a)] S. Landrock,[1] Y. P. Chiu,[2] U. Breuer,[3] and R. E. Dunin-Borkowski[1]
[1]*Peter Grünberg Institut, Forschungszentrum Jülich GmbH, 52425 Jülich, Germany*
[2]*Department of Physics, National Sun Yat-sen University, Kaohsiung 80424, Taiwan*
[3]*Zentralabteilung für Chemische Analysen, Forschungszentrum Jülich GmbH, 52425 Jülich, Germany*

(Received 20 September 2012; accepted 17 October 2012; published online 6 November 2012)

The effect of counterdoping on the Be dopant distribution in delta (δ)-doped layers embedded in Si-doped and intrinsic GaAs is investigated by cross-sectional scanning tunneling microscopy. δ-doped layers in intrinsic GaAs exhibit a large spreading, whereas those surrounded by Si-doped GaAs remain spatially localized. The different spreading is explained by the Fermi-level pinning at the growth surface, which leads to an increased Ga vacancies concentration with increasing Si counterdoping. The Ga vacancies act as sinks for the diffusing Be dopant atoms, hence retarding the spreading. © *2012 American Institute of Physics*. [http://dx.doi.org/10.1063/1.4765360]

The need of reduced power consumption and faster electronics is driving a rapid shrinking of the size of semiconductor structures. This requires an increasingly better control of the spatial distribution of dopants[1] since a future miniaturization of semiconductor structures must go hand in hand with the spatial down-scaling of doping profiles.[2] Delta (δ)-doped layers in semiconductors are a way to downscale doping profiles. However, in order to implement such downscaled doping profiles, the redistribution of impurities during growth and production processes as well as the achievable dopant concentrations needs to be understood in detail. Particularly important is a control and limitation of the spreading of initially sharp δ-doped structures at elevated growth temperatures, as the spreading affects the electronic properties of the δ-doped layer.[3] Similarly, the lateral dopant distribution within the δ-doped layer influences the carrier mobility.[4,5] Therefore, the knowledge of the actual and not just of the intended dopant positions within a δ-doped layer is a critical factor for controlling the device properties.

Experimentally most investigations of dopant distribution in δ-doped layers relied on secondary ion mass spectroscopy (SIMS) or capacitance-voltage profiling. These methods do however not provide an atomically resolved dopant mapping. A high resolution mapping of every individual dopant and its electrical properties can be achieved using cross-sectional scanning tunneling microscopy (XSTM).[6–10] XSTM dopant maps revealed Coulomb repulsions spreading the δ-doped layers[6] and auto-compensation effects limiting the achievable carrier concentration.[7,9]

However, these two observed mechanisms are only a small selection of a larger number of physical effects governing the spatial distribution of dopant atoms in δ-doped layers. Besides the simple diffusion and dopant-dopant interactions,[6,11] segregation,[11] dopant-defect interactions, dopant-surface interactions as well as a drift in electric fields[12] contribute to the spreading. On the other hand, these factors may also allow to tailor the shape of δ-doped layers. Therefore, it is of high interest to investigate the real space dopant distribution in δ-doped layers, where the spreading is tailored, e.g., by counterdoping modulating the potential within the semiconductor.

In this paper, we map the dopant atom distribution in Be δ-doped layers in GaAs embedded in Si-doped and in undoped intrinsic (i) GaAs by scanning tunneling microscopy. We observe a large spreading of the δ-doped layer surrounded by i-GaAs compared with localized δ-doped layer surrounded by Si-doped GaAs. Thus, appropriate counterdoping allows to tailor the sharpness of Be δ-doped structures. The different spreading is explained by the interaction of the Fermi-level pinning at the growth surface with the doping, giving rise to electric fields, which in turn modify the spatial distribution of Ga vacancies with increasing distance from the growth surface. The Ga vacancies act as sinks for the diffusing Be dopant atoms and hence tailor the spreading.

For our experiments, we used a GaAs structure grown by molecular beam epitaxy at a GaAs substrate temperature of $T = 500\,^{\circ}\mathrm{C}$. The epitaxial structure contained ten δ-doped layers grown by depositing $3 \times 10^{13}\,\mathrm{cm}^{-2}$ Be (or Si) dopants while the GaAs growth was interrupted. The δ-doped layers are indicated by red bars in the schematic of the growth sequence in Fig. 1. Three Be δ-doped layers (defined as type A) labelled δ_{A1} to δ_{A3} are surrounded by Si-doped GaAs (marked n in Fig. 1(b)), whereas three other Be δ-doped layers labelled δ_{B1} to δ_{B3} (type B) are embedded in i-GaAs (marked i). In addition, there is one nominally 100 nm wide Be-doped layer (marked p) surrounded by Si-doped GaAs as well as a $pnpn$-δ-doped structure in i-GaAs (layers labelled δ_{C1}, δ_{C2}, and δ_n). The Si and Be dopant distribution and levels as measured by SIMS are shown in Fig. 1(c).

Figure 1(a) shows a mosaic of constant-current STM images measured at a cleaved cross section of the epitaxial GaAs sample. The respective layers are indicated by the dashed red lines guiding the eye to the schematic diagram of the growth sequence in Fig. 1(b). The most interesting feature is that the δ-doped layers of type A (δ_{A1}, δ_{A2}, and δ_{A3}) are narrow and spatially confined. These sharp δ-doped layers are embedded in Si-doped GaAs. In contrast, the δ-doped layers of type B (δ_{B1}, δ_{B2}, and δ_{B3}), embedded in i-GaAs, exhibit a pronounced spreading, such that technically they cannot be considered as δ-doped layers anymore.

a)Electronic mail: p.ebert@fz-juelich.de.

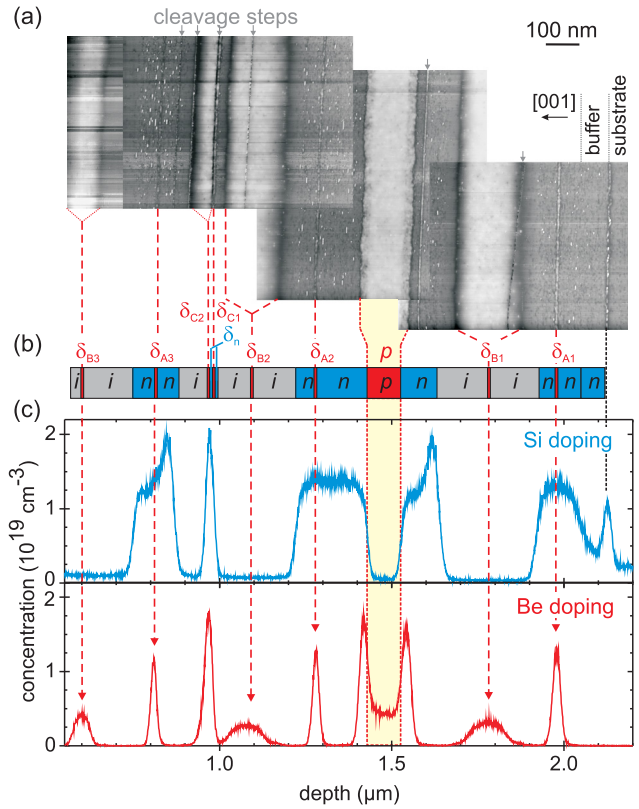

FIG. 1. (a) Mosaic of constant-current STM images showing the filled states of a cleaved cross-section of a MBE-grown epitaxial GaAs film with δ-doped layers. (b) Schematic diagram of the doping structure. (c) Concentration of Si (blue signal, upper graph) and Be (red signal, lower graph) dopants measured by SIMS. The Be δ-doped layers δ_{A1}, δ_{A2}, and δ_{A3} embedded in Si-doped GaAs are localized, while those in *i*-GaAs (δ_{B1}, δ_{B2}, and δ_{B3}) exhibit a strong widening. δ_{C1}, δ_{C2}, and δ_n mark a group of four alternating *p* and *n*-type δ-doped layers, and *p* a thick Be-doped area surrounded by Si-doped GaAs. The grey arrows indicate the positions of cleavage steps, whose height contrast was removed by shifting the *z*-scale offset of the adjacent terraces. All the remaining contrast is doping-induced.

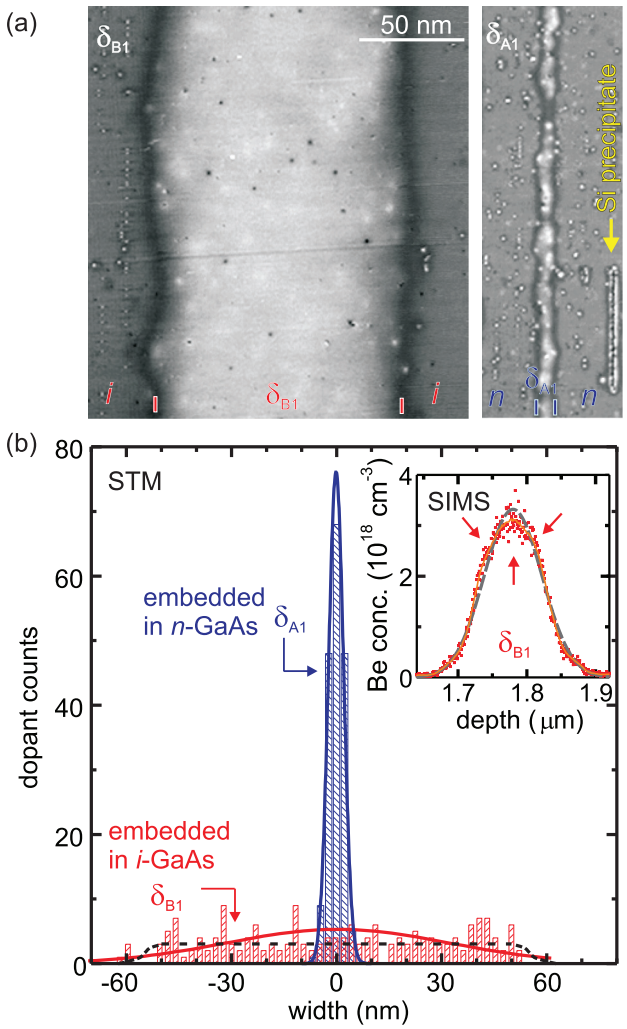

FIG. 2. (a) Filled-state STM images showing the individual dopant atoms in the δ-doped layers δ_{A1} (right) embedded in *n*-doped and δ_{B1} (left) in *i*-GaAs. The arrow marks a planar Si precipitates intersecting the cleavage surface (see Ref. 13). The dark zones represent the image of the electronic interfaces, which are marked by dashes. (b) Distribution of Be dopants in the δ-doped layers δ_{B1} (red histogram) and δ_{A1} (blue) obtained from STM images. The δ-doped layer δ_{A1} has a width of about 12 nm, whereas the Be atoms of the δ-doped layer δ_{B1} are laterally spread out over 120 nm. The solid blue and red lines are Gaussian fits to the δ_{A1} and δ_{B1} data, respectively. The dashed black line highlights the deviations of the Be distribution of the δ_{B1}-layer from a Gaussian distribution. Inset: SIMS profile of the δ-doped layer δ_{B1}. The black dashed line is a Gaussian fit to the SIMS data. The arrows mark the major deviations of the SIMS data from the Gaussian.

Nevertheless, for consistency they will be called 'δ-doped layers' in the following. In analogy, the δ-doped Be layer δ_{C1} sandwiched by two δ-doped Si layers (δ_n) in the *pnpn*-δ-doped structure (see Figure 1(a)) is narrow and sharp. In contrast, the δ-doped Be layer δ_{C2}, which is adjacent to a δ-doped Si layer (δ_n) on the right side and by *i*-GaAs on the left side, exhibits a *one-sided* spreading.

Figure 2(a) shows atomically resolved STM images of the δ-doped layers δ_{A1} and δ_{B1}. The individual dopant atoms appear a bright local contrasts about 3 to 5 nm diameter.[13] This contrast is the image of the screened Coulomb potential surrounding the negatively charged dopant atoms. The localized dark contrast features are As vacancies formed after cleavage of the surface and are thus not representative of the bulk material.[14] From such images, we deduced the distribution of Be dopants in the δ_{A1} and δ_{B1} layers by counting the individual dopant atoms as a function of their position along the growth direction. The obtained Be dopant distributions shown in Figure 2(b) are based on 184 and 180 dopant atoms observed on sections of the δ-doped layers δ_{B1} and δ_{A1} with a length of 535 nm. Based on the intensity of the imaged screened Coulomb potentials surrounding the dopant atoms, we estimate that dopant atoms up to four layers deep below the surface can be identified in the STM images.[15] Thus, the counts in the histograms correspond to an integral Be concentration in the δ-doped layers of $(4.3\pm1.0)\times10^{13}\,\mathrm{cm}^{-2}$ and $(4.2\pm1.0)\times10^{13}\,\mathrm{cm}^{-2}$, respectively. These values are in good agreement with the grown-in concentration of $3\times10^{13}\,\mathrm{cm}^{-2}$ (nominal value) and $3.5\times10^{13}\,\mathrm{cm}^{-2}$ extracted from the SIMS data. The main effect visible again in the Be dopant distributions is the extensive enlargement of layer δ_{B1} (red histogram) surrounded by *i*-GaAs compared to layer δ_{A1} sandwiched in *n*-type GaAs (blue histogram).

In the STM images, the interfaces limiting the δ-doped layers appear as a dark contrast zones. This contrast is similar to the depletion zone contrast observed in GaAs *p*-*n* junctions.[16] Hence, in analogy to the GaAs *p*-*n* junctions the dark lines represent the *electronic* interface where the Fermi energy is in midgap.[16] For the δ-doped layered embedded in

Si-doped GaAs, the electronic interfaces are very sharp and exhibit a confined dark contrast. In contrast, the interfaces of the δ-doped layers in *i*-GaAs are a wide and blurred dark zone. Since the doping level is negligible in the *i*-GaAs, the depletion zone is penetrating deep into the *i*-GaAs, giving rise to a wide electronic width of the δ-doped layer. In addition, the tip-induced band bending can also shift the dark zone toward the *i*-GaAs, widening apparently the electronic widths. This effect is more pronounced for more blunt tips such as in Fig. 1(a) (large band bending) than for atomically sharp tips (smaller band bending) as the one used in Fig. 2.

The first grown layers near the substrate are exposed longest to the growth temperature. Hence, Fig. 3 shows the width as a function of time at growth temperature. The electronic width, extracted all from the separation of the electronic interfaces in STM images in Fig. 1(a) for comparability at different times (same tip), and the width of the Be distributions (labelled dopant width) are shown as filled and empty symbols, respectively. The data corroborate the large differences in width between the δ-doped layers embedded in *i*-(type B) and in *n*-type GaAs (type A): In *n*-type GaAs, the width increases slowly from 5.3 to 11.4 nm with time at growth temperature (blue filled downward triangles and empty square). In contrast, in *i*-GaAs the δ-doped layers exhibit fast increasing electronic widths reaching for the layer δ_{B1} 170 nm. The width of the dopant distribution measured by STM and SIMS is somewhat smaller (see open circle [STM] ~120 nm and open triangles [SIMS] ~107 nm for layer δ_{B1}), but still one order of magnitude larger than for the delta-doped layers embedded in intrinsic GaAs. Furthermore, the one-sided spreaded layer δ_{C2} has a width, which fits well into the trend when multiplied by a factor of two (filled circle).

A δ-doped layer with N Be atoms broadens along the growth direction z with time t resulting in a gaussian distribution $n(z,t) = \frac{N}{\sqrt{4\pi Dt}}\exp[-\frac{z^2}{4Dt}]$ with D being the temperature dependent diffusion coefficient.[2] On this basis, the measured experimental dopant distributions were fitted by Gaussians shown as solid blue (δ_{A1}) and red (δ_{B1}) lines in Fig. 2(b). The δ-doped layer δ_{A1} is well-described by the Gaussian. However, the dopant distribution of layer δ_{B1} exhibits significant deviations from the Gaussian shape (red line). The experimental distribution is rather constant at $2.5 \times 10^{18}\,\mathrm{cm}^{-3}$ and decays only in a narrow range at the outermost edges (see dashed line serving as a guide for the eye). This is corroborated by the SIMS profile (inset of Fig. 2) showing analogous deviations from the black dashed Gaussian marked by arrows despite broadening effect due to sputter-induced roughness. The almost constant Be concentration can be related to the minimization of the repulsive screened Coulomb interactions.[6,17] If there were still a higher dopant concentration in the center of the layer, the larger interaction energy at this location would drive the dopants outward.

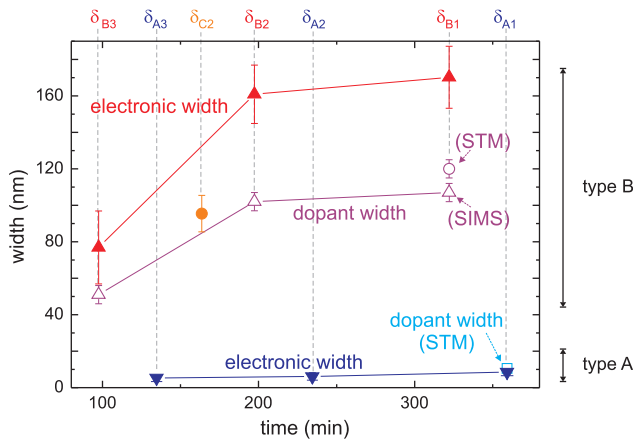

FIG. 3. Width of the δ-doped layers as a function of time at growth temperature of 500 °C. Filled triangles: electronic width defined by the separation of the electronic interfaces measured in the STM images in Fig. 1(a). Open circle and square: width of the dopant distributions of layers δ_{A1} and δ_{B1} in Fig. 2(b). Open triangles: width at half-maximum of the dopant distribution measured by SIMS. The orange filled circle represents twice the width of the layer δ_{C2} sandwiched between a Si δ-doped layer and *i*-GaAs.

In order to understand the effect of counterdoping on the spreading of the Be δ-doped layers, we consider the electronic properties of the growth surface. The GaAs(001) growth surface is usually a 2×4 reconstructed As-rich surface, where the Fermi energy is pinned in midgap.[18] A freshly grown Si-doped GaAs layer will thus initially exhibit intrinsic characteristics, which change, as the growth proceeds and the distance from the growth surface increases, towards *n*-type properties. In a static picture, the Fermi-level pinning at the growth surface induces a screening potential decaying into the bulk inducing a bending of the band edges as shown schematically in Fig. 4(b) as blue solid lines. For *i*-GaAs, the potential (red dashed lines) remains constant as the screening by free charge carriers is negligible. The screening potential in *n*-type GaAs changes the formation energy of q charged defects following $E_{Form} = E_0 + q/e(E_F - E_C)$[19,20] with e, E_C, and E_F being the electron charge, the conduction band edge, and Fermi energies, respectively. E_0 is the formation

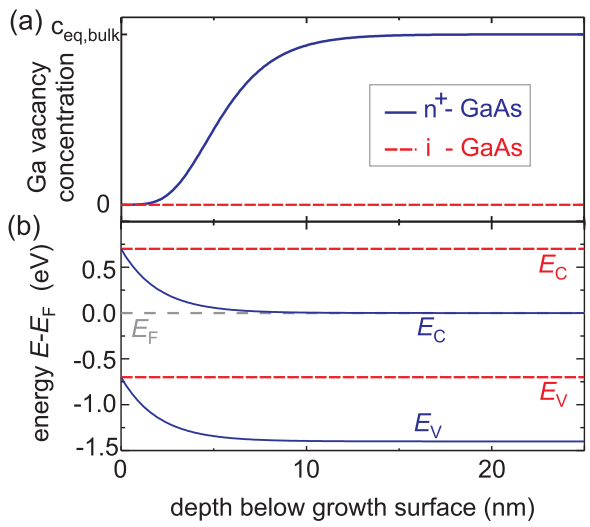

FIG. 4. (a) Concentration of triple negatively charged Ga vacancies and (b) band diagram as a function of the depth below the growth surface for *i*-GaAs (dashed red lines) and n^+-doped GaAs (blue solid lines). At the GaAs(001) growth surface, the Fermi energy is pinned in midgap. Depending on the doping, the screening by free charge carriers leads to a gradual change of the band edges until they reach their bulk values defined by the doping level. The band diagram is calculated using a screening length of 2 nm. The screening potential for n^+-doped GaAs leads to a change of the equilibrium Ga vacancy concentration shown in (a).

energy if $E_F = E_C$. The closer E_C gets to E_F with increasing depth, the more triple negatively charged Ga vacancies V_{Ga}^{3-} are formed in GaAs by the process $Ga_{Ga} \rightarrow V_{Ga}^{3-} + Ga_i^+ + 2h^+$.[13,21] The depth dependence of the vacancy concentration $c_V(z) \sim \exp(E_{Form}(z)/kT)$ (Boltzmann constant k) is shown as solid blue line in Fig. 4(a). Other defects have a higher defect formation energy[20,22] and hence a negligible concentration. The build-in electric field attracts the positively charged Ga interstitials Ga_i^+ toward the surface[23] where they are incorporated. The remaining V_{Ga}^{3-}, however, influence the diffusion of the Be dopants.

Be dopants diffuse in GaAs through a substitutional-interstitial process $Be_{Ga}^- \leftrightarrow V_{Ga}^{3-} + Be_i^+ + 2h^+$, since only Be on interstitial sites Be_i^+ is highly mobile at growth temperatures.[24] The V_{Ga}^{3-} act as sinks for Be_i^+, hence immobilizing the Be atom. Thus with increasing V_{Ga}^{3-} concentration, the diffusion of Be is retarded. Be only diffuses freely in intrinsic GaAs with negligible V_{Ga}^{3-} concentration, whereas in highly n-doped GaAs with high V_{Ga}^{3-} concentration the diffusion is small. This explains the different spreading of Be δ-doped layers in intrinsic and n-type GaAs, providing a path of tailoring the desired dopant distribution.

Finally, previous STM measurements of Be,[6] C,[10] or Si[8] δ-doped layers in GaAs exhibit a much smaller broadening of the δ-doped layers. This effect is due to the lower growth temperature of 480 °C used in Refs. 6 and 8 than our 500 °C (Be doping) and due to the lower diffusivity of Si and especially C in GaAs.[10] Our samples were purposely grown to increase diffusive spreading through larger growth temperatures and higher dopant concentrations, to highlight the effect of counterdoping.

In conclusion, we mapped the dopant distribution in Be δ-doped layers embedded in Si-doped and in intrinsic GaAs by scanning tunneling microscopy. We observe a large spreading of δ-doped layers in i-GaAs compared to localized δ-doped layers surrounded by Si-doped GaAs. The different spreading is explained by the interaction of the Fermi-level pinning at the growth surface with the doping, giving rise to electric fields. These induce the formation of Ga vacancies, which retard the Be diffusion by being sinks for the diffusing interstitial Be atoms. Hence, counterdoping can be used to tailor the sharpness of Be δ-doped structures.

The authors thank K. H. Graf for technical support, Ch. Krause for the sample growth, and the National Science Council of Taiwan for financial support under Grant No. 101-2918-I-110-001.

[1]S. Roy and A. Asenov, Science **309**, 388 (2005).
[2]E. F. Schubert, *Delta-Doping of Semiconductors* (Cambridge University, Cambridge, 1996).
[3]A. Zrenner, F. Koch, and K. Ploog, Surf. Sci. **196**, 671 (1988).
[4]A. F. J. Levi, S. L. McCall, and P. M. Platzman, Appl. Phys. Lett. **54**, 940 (1989).
[5]J. M. Shi, P. M. Koenraad, A. F. M. van de Stadt, F. M. Peeters, G. A. Farias, J. T. Devreese, J. H. Wolter, and Z. Wilamowski, Phys. Rev. B **55**, 13093 (1997).
[6]M. B. Johnson, P. M. Koenraad, W. van der Vleuten, H. Salemink, and J. Wolter, Phys. Rev. Lett. **75**, 1606 (1995).
[7]B. Grandidier, D. Stiévenard, J. P. Nys, and X. Wallart, Appl. Phys. Lett. **72**, 2454 (1998).
[8]S. Modesti, D. Furlanetto, M. Piccin, S. Rubini, and A. Franciosi, Appl. Phys. Lett. **82**, 1932 (2003).
[9]S. Modesti, R. Duca, P. Finetti, G. Ceballos, M. Piccin, S. Rubini, and A. Franciosi, Phys. Rev. Lett. **92**, 086104 (2004).
[10]L. Winking, M. Wenderoth, T. C. G. Reusch, R. G. Ulbrich, P.-J. Wilbrandt, R. Kirchheim, S. Malzer, and G. Döhler, J. Vac. Sci. Technol. B **23**, 267 (2005).
[11]E. F. Schubert, J. M. Kuo, R. F. Kopf, H. S. Luftman, L. C. Hopkins, and N. J. Sauer, J. Appl. Phys **67**, 1969 (1990).
[12]E. F. Schubert, J. M. Kuo, R. F. Kopf, A. S. Jordan, H. S. Luftman, and L. C. Hopkins, Phys. Rev. B **42**, 1364 (1990).
[13]C. Domke, Ph. Ebert, M. Heinrich, and K. Urban, Phys. Rev. B **54**, 10288 (1996).
[14]Ph. Ebert, M. Heinrich, M. Simon, K. Urban, and M. G. Lagally, Phys. Rev. B **51**, 9696 (1995).
[15]Ph. Ebert, Surf. Sci. Rep. **33**, 121 (1999).
[16]N. D. Jäger, M. Marso, M. Salmeron, E. R. Weber, K. Urban, and Ph. Ebert, Phys. Rev. B **67**, 165307 (2003).
[17]Ph. Ebert, T. J. Zhang, F. Kluge, M. Simon, Z. Y. Zhang, and K. Urban, Phys. Rev. Lett. **83**, 757 (1999).
[18]H. Lüth, *Solid Surfaces, Interfaces and Thin Films* (Springer, Heidelberg, 2010).
[19]T. Y. Tan, H. M. You, and U. M. Gösele, Appl. Phys. A **56**, 249 (1993).
[20]J. E. Northrup and S. B. Zhang, Phys. Rev. B **47**, 6791 (1993).
[21]T. Y. Tan and U. Gösele, Appl. Phys. Lett. **52**, 1240 (1988).
[22]G. A. Baraff and M. Schlüter, Phys. Rev. Lett. **55**, 1327 (1985).
[23]D. G. Deppe, Appl. Phys. Lett. **56**, 370 (1990).
[24]S. Yu, T. Y. Tan, and U. Gösele, J. Appl. Phys. **69**, 3547 (1991).